POLITECNICO DI TORINO
Repository ISTITUZIONALE

Melting of PCM in a thermal energy storage unit:
Numerical investigation and effect of nanoparticle

(Article begins on next page)

25 August 2022

MELTING OF PCM IN A THERMAL ENERGY STORAGE UNIT: NUMERICAL INVESTIGATION AND EFFECT OF NANO-PARTICLES ENHANCEMENT

Adriano Sciacovelli*
Department of Energy
Politecnico di Torino, Italy
adriano.sciacovelli@polito.it

Francesco Colella
Department of Energy
Politecnico di Torino, Italy
francesco.colella@polito.it

Vittorio Verda
Department of Energy
Politecnico di Torino, Italy
vittorio.verda@polito.it

* Corresponding author. Tel.: +39 011 564 4478; fax : +39 011 564 4499. E-mail address: adriano.sciacovelli@polito.it

Abstract

The present paper describes the analysis of the melting process in a single vertical shell-and-tube LHTES unit and it is directed at understanding the thermal performance of the system. The study is realized using a computational fluid-dynamic (CFD) model that takes into account of the phase change phenomenon by means of the enthalpy method. Fluid flow is fully resolved in the liquid PCM in order to elucidate the role of natural convection. The unsteady evolution of the melting front and the velocity and temperature fields is detailed. Temperature profiles are analyzed and compared with experimental data available in the literature. Other relevant quantities are also monitored, including energy stored and heat flux exchanged between PCM and HTF. The results demonstrate that natural convection within PCM and inlet HTF temperature significantly affect the phase change process.

Thermal enhancement through the dispersion of highly conductive nano-particles in the base PCM is considered in the second part of the paper. Thermal behavior of the LHTES unit charged with nano-enhanced PCM is numerically analyzed and compared with the original system configuration. Due to increase of thermal conductivity augmented thermal performance are observed: melting time is reduced of 15% when nano-enhanced PCM with particle volume fraction of 4% is adopted. Similar improvements of the heat transfer rate are also detected.

Keywords: PCM, Thermal energy storage, CFD, Natural convection, Phase change, Nano-particles

NOMENCLATURE

A_{mushy}	Mush zone constant [kg/(m^3 s)]
c_p	Specific heat [J/(kg K)]
C	Constant Eq. (13)
d_p	Particle diameter (m)
D	Diameter (m)
$\vec{g}$	Gravity acceleration (m/s^2)
h	Specific enthalpy (J/kg)
H	Height (m)
h_{ref}	Reference specific enthalpy (J/kg)
k	Thermal conductivity [W/(m K)]
L	Specific latent heat (J/kg)
$\dot{m}$	Mass flow rate (kg/s)
p	Pressure (Pa)
R_t	Thermal resistance [(m^2 K)/W]
r	Radial coordinate (m)
$\vec{S}$	Momentum source term (Pa/m)
T	Temperature (K)
T_g	Inlet temperature (K)
T_m	Melting temperature (K)
T_0	Reference temperature (K)
$\vec{V}$	Velocity vector (m/s)
x	Axial coordinate (m)
Greek letters	
β	Thermal expansion coefficient (1/K)
γ	Liquid fraction
ε	Thermal storage efficiency
ϵ	Computational constant, Eq. (6)
μ	Dynamical viscosity (Pa s)
ρ	Density (kg/m^3)
φ	Particle volume fraction
Dimensionless	
Re	Reynolds number, $\mathrm{Re} = \rho V D / \mu$
Ste	Stefan number, $\mathrm{Ste} = c_p (T_g - T_m)/L$
Ra	Rayleigh number, $\mathrm{Ra} = g \beta \rho^2 c_p (T_g - T_m) R^3 / (\mu k)$

1. Introduction

Thermal energy storage plays a key role when it is necessary to store excess energy that would be otherwise wasted and to match demand and supply. This is an important problem in renewable

energy systems and cogeneration systems. Energy storage techniques can be classified in three main groups: sensible, latent and thermo-chemical heat storage. Latent heat thermal energy storage (LHTES) systems are becoming increasingly attractive because of the high energy storage density and the possibility of storing and delivering latent heat at nearly constant temperature, corresponding to the phase transition temperature of the phase change material (PCM). On the other hand, one of the main disadvantages is the low thermal conductivity of many PCMs, causing poor melting and solidification rates. Therefore the advance of LHTES requires the understanding of heat transfer in the PCM during the phase transition.

A wide range of studies on PCMs and LHTES system have been conducted by various researchers, including analytical, experimental and numerical investigations. Different geometrical configurations have been proposed for the PCM enclosures: spherical shells, tall rectangular enclosures and cylindrical pipes [1]. Various authors have investigated melting process in vertical circular pipes since this configuration is closer to real PCM heat exchangers applications. Sparrow and Broadbent [2] experimentally investigated the melting of a paraffin in a metal tube placed in a constant-temperature bath. Liquid fraction evolution was observed by stopping the phase-change process at different instant of times and removing solid PCM from the tube. The influence of temperature difference between the tube wall and the paraffin was also investigated. The authors pointed out that natural convection has a relevant effect on the melting process since the observed melting front presented a typical conical shape. Mennon et al. [3] performed the experimental analysis of PCM melting in vertical pipes. The study involved a commercial paraffin wax and copper tubes, moreover various quantities of PCM were considered. Mennon et al. [3] also highlighted the effects of natural convection by tracing fluid motion of liquid PCM. Melting in a vertical cylinder have been also conducted by Jones [4] who observed a non-negligible effect of the buoyancy on the process. Indeed, melt front thickness was observed to vary along the vertical direction. Experimental measures of melting front positions by sophisticate image processing and temperatures recording were also used to validate numerical computations performed by the same authors.

Zhang and Bejan [5] experimentally studied the time-depending melting of *n*-octadecane in a tall enclosure. Although geometry and boundary conditions are different, this configuration has some peculiar features similar to those observed in vertical tubes. Zhang and Bejan [5] also developed an analytical model which correctly predicts experimental values of overall Nusselt number. Similarly, Pal and Joshi [6] analyzed the melting process inside a side-heated tall enclosure filled with *n*-triacontane. The authors experimentally studied the phenomenon and they recorded time evolution of PCM temperature and melt front shape. Pal and Joshi [6] also performed a numerical study of the process showing good agreement with the experimental melting fronts. The authors also proposed correlations for liquid fraction and heat transfer rate that can be used for design purposes.

Sari and Kaygusuz [7] investigated the performance of a cylindrical shell-and-tube latent heat storage system. In this configuration the PCM fills the shell while the heat transfer fluid (HTF) flows inside a single tube and therefore heat transfer takes place between the working fluid and the PCM. The authors observed solid-liquid interface evolution, temperature distribution and heat flux. Sari and Kaygusuz [7] pointed out that heat flux is largely influenced by natural convection in liquid PCM. Keles et al. [8] considered a mixture of lauric and myristic acids as phase change material. The authors experimentally established the thermal performance of the PCM in a vertical shell-and-tube heat storage system. Keles et al. [8] evaluated the effect of HTF inlet conditions on

melting and solidification processes. The authors concluded that a mixture of lauric and myristic acids is particularly suitable for low-temperature solar energy storage applications.

Ettouney et al. [9] studied heat transfer characteristic of PCM in a vertical shell-and-tube configuration. Several thermocouples were placed in the phase change material in order to provide detailed temperature measurements during melting and solidification processes. The authors also investigated the influence of operating conditions. In particular the results of Ettouney et al. [9] indicates that melting is dominated by natural convection for upward flow of the heat transfer fluid. However when HTF was allowed to flow downward in the unit melting process was found to be dominated by conduction. Akgun et al. [10] experimentally analyzed melting and solidification of paraffin in a vertical tube in shell heat exchanger system. The thermophysical properties of the paraffin were obtained through differential scanning calorimeter analysis. Akgun et al. [10] also investigated the effect of the inlet temperature and the mass flow rate of the HTF on the melting and solidification processes. Aydin et al. [11] suggested a novel modification of the shell-and-tube geometry: the authors proposed an inclined outer surface of the shell in order to enhance heat transfer. Aydin et al. [11] experimentally investigated the proposed geometry considering a paraffin wax as PCM. The authors found a 40% reduction in the total melting time for a shell inclination in the range of 5-15°.

A relevant part of literature is dedicated to the modelling of LHTES systems and related phase change problems. The most common methods are the equivalent capacity method and the enthalpy method. The latter was proposed and then extended by several authors [12-14]. When the enthalpy method is used, energy equation is written in terms of total volumetric enthalpy which is the sum of both sensible and latent heats. Moreover, the regions where solid and liquid phases coexist they are treated as an equivalent porous medium with the liquid fraction acting as porosity. By introducing the enthalpy method, the phase-change problem is significantly simplified since the governing equation is the same for both liquid and solid phase. Therefore the necessity of explicitly tracking solid-liquid boundaries is avoided.

An enthalpy based formulation has been employed by Lacroix [15] who developed a 2D numerical model to analyze the behaviour of a cylindrical storage system with n-octadecane. Fluid flow was not solved inside the liquid PCM and the effect of natural convection was taken into account by means of empirical correlations for the PCM thermal conductivity. Ismail and Abugderan [16] performed the numerical analysis of a vertical shell-and-tube LHTES system. The authors determined the velocity field inside the HTF fluid and they assumed conduction heat transfer to be dominant in the PCM region. Consequently the flow field due to buoyancy was not solved. Trp [17] also adopted the enthalpy formulation to solve the energy equation coupled with the thermo-fluid-dynamic model of the HTF. Ismail and Melo [18] numerically studied the problem of fusion of PCM in a shell-and-tube unit in the presence of natural convection. The authors employed a 2D model of a meaningful portion of the complete system, however they did not numerically solve the flow field of the HTF. Trp et al. [19] performed a numerical and experimental investigation on both melting and solidification in a shell-and-tube LHTES unit. The authors adopted the enthalpy method to solve governing equations for PCM and HTF. The results of the investigation indicate that phase change and HTF forced convection must be treated as a conjugate problem. Furthermore Trp et al. [19] pointed out that operating conditions, unit length and outer tube radius must be chosen carefully since they affect significantly the heat transfer rate. More recently Shmueli et al. [20] investigated the melting process in a vertical tube. The authors coupled the enthalpy method with the volume-of-fluid model in order to take into account of PCM volume change during

melting. The numerical result were compared to previous experimental data by means of image processing technique. In addition the effect of various numerical schemes and parameters on the results were investigated.

In spite of relative merits, PCMs possess low thermal conductivity, this leads to low melting/solidification rates which is a major drawback for large scale applications of latent heat storage. Various techniques have been proposed to enhance thermal performance of PCMs; among the others, the use of extended surfaces [21] and highly conductive PCM-graphite composites [22,23] have been quite successful. Only a limited number of studies have been conducted on the dispersion of high thermal conductivity particles in the PCM: Mettawee and Assassa [24] investigated the thermal response of paraffin wax with aluminium powder dispersed into it. The experiments were conducted on a compact PCM solar collector. The solar energy was stored in the PCM and discharged to water flowing in pipes embedded in the PCM. Mettawee and Assassa [24] studied both melting and solidification process and found a reduction of 60% of the melting time when aluminium powder was added to the PCM. Khodadadi and Hosseinizadeh [25] numerically studied the water solidification in differentially-heated square cavity. Khodadadi and Hosseinizadeh [25] treated the nanofluid as a continuum media with thermal equilibrium between water and solid nanoparticles. The authors found that the addition of copper nanoparticles to the water can bring a reduction of solidification time up to 50%. Ho and Gao [26] prepared n-octadecane with embedded alumina nano-particles and its thermophysical properties were experimentally analyzed. The authors reported relative enhancement in effective thermal conductivity and an increase of the effective dynamical viscosity. Seeniraj et al. [27] also reported relevant performance improvements during melting by means of nano-particles addition to pure PCM. However, Seeniraj et al. [27] considered very high particle volume fractions up to 60%: experiments conducted by Fan and Khodadadi [28] showed that particles sedimentation may occur even when much lower concentrations are considered. Consequently, thermal enhancement due to dispersion of nano-particles is also reduced.

In this context, the present work aims at investigating the melting process of pure PCM inside vertical cylindrical shell-and-tube system and the effect of nanoparticles dispersion into the base PCM. In this study the complete set of conservation equations for the melting process is solved and the buoyancy-driven fluid motion within the melted PCM is explicitly computed. No a priori assumptions are used about the influence of natural convection on the phase change. Moreover the heat transfer problem in the PCM domain is fully coupled with the thermo-fluid-dynamic problem of HTF. Temperature, velocity and phase fields are obtained and analyzed as functions of time showing the evolution of the heat transfer in the system. Furthermore the numerical results are compared with experimental data available in the literature. The effects of inlet mass flow rate and temperature on the melting process are evaluated and presented. The effect of using copper nano-particles as thermal conductivity enhancer is also analyzed by means of a computational study. In particular, performance improvements are investigated for different particle volume fractions and compared with the original system configuration.

2. Mathematical Model

2.1 System description

The system here under investigation has been experimentally analyzed by Akgun et al. [10]. It consists of a vertically orientated single shell and tube LHTES device, as shown in Figure 1. Water circulates inside the inner tube and acts as HTF. The PCM is placed in the gap between the HTF tube and the outer shell. A commercial paraffinic wax from MERCK company is used as phase change material. Several thermocouples have been used by Akgun and coworkers to monitor the temperature inside the PCM during the phase change. Further measurements include the HTF inlet and outlet temperature. Finally the HTF mass flow is measured by a rotameter. Different scenarios are considered by varying the inlet temperature and mass flow rate. Figure 1 illustrates the geometrical dimensions of the system and the locations of thermocouples.

Initially the external shell of Figure 1 contains solid PCM at a temperature T_i lower than the melting temperature T_m. At time $t > 0$, a water mass flow rate starts to flow through the inner pipe. The water inlet temperature is held at a constant value (T_g), such that $T_g > T_m$. The resulting heat flux conducted through the pipe wall causes PCM melting. The melting process is completed when PCM is completely liquid.

2.2 Governing equations

The governing equations for the transient analysis of PCM melting process include Navier-Stokes equation, the continuity equation and the energy equation. Density variation due to phase change is neglected; the Boussinesq approximation is applied. Thus density change within the liquid PCM which drives natural convection in the liquid phase is considered in the body force terms. Accordingly, the governing equations used here for the PCM are [4]:

Continuity:

$$\frac{\partial \rho}{\partial t} + \nabla \cdot (\rho \vec{V}) = 0 \tag{1}$$

Momentum:

$$\rho \frac{\partial \vec{V}}{\partial t} + \rho (\vec{V} \cdot \nabla)\vec{V} = -\nabla p + \mu \nabla^2 \vec{V} + \rho \vec{g}(T - T_0) + \vec{S} \tag{2}$$

Energy:

$$\frac{\partial}{\partial t}(\rho h) + \nabla \cdot (\rho \vec{V} h) = \nabla \cdot (k \nabla T) \tag{3}$$

where ρ is the density, $\vec{V}$ is the velocity of the liquid PCM, p is the pressure, μ is the dynamic viscosity, $\vec{g}$ is the gravity vector, β is the thermal expansion coefficient, T_0 is the reference temperature and $\vec{S}$ is the momentum source term. In order to deal with the phase change problem, the enthalpy-porosity approach has been used since it does not require and explicit tracking of the solid-liquid interface [14]. The presence of the solid or liquid phase is instead monitored by using a quantity known as liquid fraction. Accordingly the enthalpy h in Eq. (3) is expressed as

$$h = h_{ref} + \int_{T_{ref}}^{T} c_p \, dT + \gamma L \qquad (4)$$

where h_{ref} is the enthalpy at the reference temperature T_{ref}, L is the latent heat and γ is the liquid fraction. The latter is defined as:

$$
\begin{aligned}
\gamma &= 0 && \text{if} && T < T_{solidus} \\
\gamma &= 1 && \text{if} && T > T_{liquidus} \qquad (5) \\
\gamma &= \frac{T - T_{solidus}}{T_{liquidus} - T_{solidus}} && \text{if} && T_{solidus} < T < T_{liquidus}
\end{aligned}
$$

The enthalpy-porosity formulation treats different phases as a porous media by means of the following momentum source term $\vec{S}$:

$$\vec{S} = \frac{(1-\gamma)^2}{(\gamma^3 + \xi)} A_{mushy} \vec{V} \qquad (6)$$

where ξ is a small number typically around 10^{-3} introduced to avoid the division by zero and A_{mushy} is the mushy zone constant which describe how steeply the velocity are reduced to zero when the material solidifies. The latter is usually a very large number, ranging between 10^4 to 10^8 kg/(m^3 s). The effect of mushy zone constant has been investigated by Shmueli et al. [20]: they numerically studied the melting process of Rubitherm paraffin in a open vertical cylinder including the effect of PCM density variation by means of Volume-of-Fluid model. They found that a value of 10^8 kg/(m^3 s) allows to achieve the best match between their numerical results and experimental data. In this paper the PCM volume change due to melting is neglected and the paraffin wax used in the experiments by Akgun et al. [10] was obtained from MERCK company. Moreover experimental time evolution of liquid fraction and of solid PCM shape is not available from [10]. Thus the influence of A_{mushy} cannot be fully evaluated for the problem investigated in this paper. Consequently the value of A_{mushy} used here for the computations is the standard one, i.e. 10^5 kg/(m^3 s). The thermophysical parameters adopted in the model are summarized in Table 1.

The thermo-fluid-dynamic behaviour of the HTF has been modelled using the classical Navier-Stokes equation and energy equation. As illustrated later in the paper HTF flow is turbulent, thus an appropriated turbulence model is required. In this work the standard *k-epsilon* model is adopted. It has been shown [4,29] that Prandtl, Rayleigh, Stefan, Subcooling, Darcy and Fourier are the dimensionless numbers that govern the melting problem in the PCM. In the present work the attention is focused on the effect of Rayleigh and Stefan numbers. In the following analysis *Ra* and *Ste* numbers are based on the inlet HTF temperature [16,18]. Furthermore Reynolds number is also considered because of the HTF flow.

When the addition of nano-particle is considered, thermal properties of PCM-particles mixture must be properly computed. In this study density, specific heat, latent heat and Boussinesq term are determined in the following way [25]:

$$\rho = (1-\phi)\rho_{PCM} + \phi \rho_p \qquad (7)$$

$$\rho c_p = (1-\phi)(\rho c_p)_{PCM} + \phi(\rho c_p)_p \qquad (8)$$

$$\rho L = (1-\phi)(\rho L)_{PCM} \qquad (9)$$

$$\rho\beta = (1-\phi)(\rho\beta)_{PCM} + \phi(\rho\beta)_p \qquad (10)$$

where ϕ is volume fraction of particles; subscripts PCM and p stand for PCM bulk properties and solid particles properties. Effective dynamic viscosity is evaluated by means of Brinkmann relation [30]:

$$\mu = \frac{\mu_{PCM}}{(1-\phi)^{2.5}} \qquad (11)$$

The effective thermal conductivity for the PCM – particles mixture is obtained by means of the following relation [31]:

$$\frac{k_{eff}}{k_{PCM}} = \frac{k_p + 2k_{PCM} - 2\phi(k_{PCM} - k_p)}{k_p + 2k_{PCM} + \phi(k_{PCM} - k_p)} \qquad (12)$$

where the subscript eff stands for effective. The contribution due the thermal dispersions is considered as follow [25]:

$$k_d = C\rho c_p \left|\vec{V}\right|\phi d_p \qquad (13)$$

where d_p is the particle diameter and subscript d stands for dispersion effect. Therefore the overall thermal conductivity is obtained as follow:

$$k = k_{eff} + k_d \qquad (14)$$

2.3 Boundary and Initial Conditions

At time $t = 0$ the PCM is taken to be motionless solid and at the temperature of 25°C. For the melting process three different values of water inlet temperature have been considered: $T_g = 60, 70$ and 75°C. Three different water mass flow rates are examined: $\dot{m} = 8, 12$ and 16 kg/min. No slip boundary condition is imposed on solid walls. Furthermore, on the pipe outlet cross section pressure is set equal to ambient pressure and the outer shell of the LHTES system is considered as adiabatic. The cases considered in this work are summarized in Table 2.

2.4 Numerical Approach

The modeling has been conducted by means of finite-volume technique. The commercial software Fluent® has been used. In this particular application a segregated solver has been adopted to address the problem and SIMPLE algorithm has been used to solve the pressure-velocity coupling. Furthermore, the LHTES system geometry allows to adopt a 2D axial-symmetric model.

The convective fluxes have been approximated by using a second order upwind scheme. Second order implicit time integration scheme has been employed. Time step of 0.05s has been used to obtain time-step independent solutions. A structured grid of 23500 cells was found to be sufficient to achieve grid independence. The number of grid nodes are 50 and 470 in the x and r directions, respectively. An iterative time-advancement scheme has been employed where all the equations are

solved iteratively in a segregated mode, until the convergence criteria are met. The convergence criteria are set as the relative residual of all variables, including mass, velocity components and temperature less than 10^{-6}, for each time step.

3. Numerical Results

3.1 Flow Structure

The thermo-fluid-dynamic behavior of the LHTES system is presented in this section. Since different scenarios are considered, for sake of simplicity a detailed analysis of the CFD results is presented for Case I which is characterized by a HTF mass flow rate of 8 kg/min and $T_g = 60°C$ (accordingly Re = 6044, Ste = 0.15 and Ra = 2.63x10^7). This case is also used to empirically validate the model against the experimental results of Akgun et al. [10].

Figure 2 presents the HTF velocity magnitude contours computed by the CFD model. The velocity profile shows that fully developed flow is established at a distance of about 0.15 m from the inlet. This finding confirms, as already pointed out in [17], that the adoption of empirical correlations for heat transfer in fully developed flow conditions may results in significant error for the evaluation of the system performance, especially for short LHTES systems. Figure 3 illustrates the time evolution of the melting front in the PCM. As pointed out by Jany and Bejan [32] the process consists of a sequence of different regimes: immediately after $t = 0$ the melting process is ruled by pure conduction. Initial PCM temperature is only 12.8°C below melting temperature range; consequently HTF pipe wall is quickly wrapped by a thin layer of liquid PCM as can be observed in the first contour of Figure 3. In this very initial phase of melting process, the melt front thickness is constant along the entire length. However, rapidly melting becomes more evident in the top zone of the LHTES system. At time $t = 2000$ s and $x = 0.45$ m, melted PCM has already reached the outer wall, while in the bottom part of the shell the melted PCM fraction is negligible. During this second regime of the melting process, i.e. the mixed conduction plus convection regime [32], buoyancy-driven currents play an important role in the upper part of the system while conduction is still dominant in the bottom part of the system. Indeed melt thickness is still small for an axial coordinate x less than 0.3 m while the largest variation of melt thickness occurs in a relatively small portion of the cylinder. Moreover, melt front assumes the typical conical shape that has been observed by several authors [2,4,5]. It is interesting to notice that the largest variation of melt thickness occurs in a relatively small portion of the cylinder, this phenomenon is connected with the aspect ratio H/D; large aspect ratio inhibits convective currents, while when low H/D values are adopted melt layer thickness can vary along the entire length [18]. During the last stage of the process, that is the convection regime [32], buoyancy becomes relevant also in the lower part of the unit, consequently melt thickness increases as can be observed in Fig. 3 at time $t = 6000$ s.

Streamlines at four different times are given in Figure 3. At the early stage of the melting process no appreciable fluid flow is established in the PCM. However, as the melting process progresses, natural convection is established in the liquid PCM. At t = 2000 s, a vortex is found in the zone where most part of melt thickness variation occurs. This fluid dynamic structure is peculiar of melting in vertical cylinders and tall enclosures and it has been observed by different researchers [4,6]. Such vortex structure promotes PCM melting since it enhances the heat transfer between the hot HTF pipe wall and the solid-liquid interface; thus natural convection plays a major role during

the melting process. From streamlines distribution it is also possible to observe that buoyancy is not particularly marked where liquid PCM has already reached the outer pipe.

Temperature distribution is shown in Figure 4. In absence of natural convection, i.e. at t = 240 s, the melting process is controlled by thermal-diffusion consequently temperature contours are aligned with the *x*-axis. As the buoyancy starts to affect the melting process, thermal stratification can be noticed. Vertical temperature gradients are observed in the proximity of the region where the vortex is located. Where PCM melting is completed, further energy is stored as sensible heat. Consequently liquid PCM temperature raises up to HTF inlet temperature, since the system is considered adiabatic.

3.2 Comparison between numerical predictions and experimental data

Time-dependent variations of computed temperature and the experimental results obtained by Akgun et al. [10] are compared in Figure 5: sufficient agreement is achieved in the details of the melting process. Initially the PCM is cooled down and the solid phase is heated until melting temperature range is reached. Each plot reported in Fig. 5 shows a sharp temperature increase at different time frames, depending on the considered position. This phenomenon is due to the passage of the melting front through the thermocouple position. Better agreement is observed between predictions and measurements in the upper portion of the system where melting begins earlier, as confirmed by the experimental values of T_{61} and T_{51}. Some discrepancies are found between numerical and experimental values of T_{31} and T_{41} in the range 0 − 100 min, namely during the PCM heating from initial temperature to melting range. The experimental plots of T_{31} and T_{41} show a smooth trend while the corresponding numerical values present a more rapid increase. In the lower portion of the system PCM melting occurs between 200 and 250 min as confirmed by numerical and experimental values of T_{11} and T_{21}. These temperature show a flat profile before melting takes place. This indicates that heat conduction is relevant in the bottom of the LHTES for most of the melting process. The temperatures T_{11} and T_{21} predicted at the end of melting process differ from the corresponding experimental values. This can be attributed to heat losses through the side wall, with this effect being more accentuated for the thermocouple T_{11} which is placed exactly on the boundary.

Figure 6 presents a comparison between experimental and numerical predictions, allowing for better performance assessment of the numerical model. Given the time-dependent nature of the process, experimental data and numerical predictions at each thermocouple location have been compared at 4 different times equally spaced during the time span 0 − 200 min of the melting process. The data are presented as dispersion plots having on the *x*-axis the experimental measurements and on the *y*-axis the numerical predictions. The plot also contains two ±30% deviation lines on a °C temperature scale. A general overview of the plot confirms that the numerical model is able to predict the experimental data within a 30% error on a °C temperature scale. Largest deviations are observed for temperature T_{21}; indeed numerical model overestimates T_{21} of about 6°C during the early stage of the melting process as illustrated in Fig. 5. Moreover measurements show a increase of temperature T_{21} while the numerical model predicts a flat profile of such temperature in the time range 0 − 150 min. The dispersion plot confirms that the numerical predictions are more precise for thermocouple placed in the upper part of the unit, that is T_{51} and T_{61}. For such temperatures numerical predictions and experimental values differs of about 3°C. Moreover numerical results are generally more

accurate during the last stage of melting process when liquid PCM is heated up and sensible heat is stored in the unit.

3.3 Parametric study

In order to assess the role of HTF inlet conditions, several cases have been studied as summarized in Table 2. Three cases with different Reynolds number have been considered by varying the HTF mass flow rate. Rayleigh and Stefan numbers have been kept unchanged for these three cases of Table 2. The authors observed that for turbulent flow of the HTF Reynolds number does not affect the heat transfer process which is dominated by conduction and natural convection at PCM side. Similar results have been also reported in [33]. This phenomenon is particularly accentuated because of the poor thermal properties of the PCM, namely the low thermal conductivity. However, as pointed out by Adine [33] Re number can affect melting rate if laminar regime is considered.

Different Ra and Ste numbers have been considered in order to understand the effect of HTF inlet temperature on the temporal evolution of the liquid fraction in the unit. In order to isolate the effects due to Ra and Ste numbers, in cases IV and V of Table 2 the Reynolds number is kept constant and equal to 6044. Rayleigh and Stefan numbers can be only varied independently by properly adjusting ΔT and D. This means that different sizes of the LHTES system should be considered. In the work here presented the size of the device is kept constant, thus in not possible to fully uncouple the effects of Ra and Ste numbers. Figure 7 illustrates how an increase in inlet HTF temperature lead to a shorter melting time. Accordingly to the definition of Rayleigh and Stefan numbers, a larger HTF inlet temperature also corresponds to larger Ra and Ste non-dimensional groups. The plot shows that for case V melting rate is considerably shorter than for case I. In particular it can be observed that an increase of 15°C of HTF inlet temperature induces a 38% reduction of melting time.

Figure 8 depicts the time wise variation of sensible and latent energy stored in the LHTES system for different HTF inlet temperatures; for all the cases reported in Fig. 8 Re number is 6044. During the early stages of the process sensible and latent heat are comparable; following this stage the amount of energy stored as latent heat becomes predominant as can be appreciated from Fig. 8. Towards the end of melting process, PCM is almost completely liquid and latent heat storage rate decreases as can be observed from the slope of curves reported in Fig. 8. During the final stage of the process liquid PCM is heated up and therefore sensible heat is accumulated in the unit. In Case I latent heat represents the 75% of the overall stored energy once melting is completed. The amount of sensible energy stored increases when higher inlet HTF temperature occurs. Indeed, for Case III latent heat is 67% of the total energy stored in the unit.

Interesting considerations can be drawn by comparing the energy storage density of traditional water storage systems with the present LHTES unit. The size of the traditional water storage systems has been computed under the assumption of storing the same amount of energy accumulated in the LHTES unit. The analysis shows that an energy density of about 250 MJ/m^3 can be achieved with the latent heat storage unit while traditional water system allows to obtain an energy density of 83MJ/m^3. Therefore a clear advantage of using latent heat systems is the possibility of significantly decrease the size of the storage unit.

Faster melting is due to higher heat flux exchanged through the HTF pipe wall, as shown in Figure 9. In Case I, after an initial decrease, the heat flux is nearly constant in the range 15 – 100 min. This behavior is due to natural convection flow that enhances heat transfer between solid PCM and HTF. Therefore, in such lapse of time the melting process proceeds with a constant rate. For Cases IV and

V an initial higher average heat flux occurs. Consequently, a corresponding steeper curve can be seen in Figure 7. However, for Cases IV and V the heat flux start to rapidly decrease after t = 50 min.

The average thermal resistance is depicted in Figure 10. Such quantity has been defined as $R_t = (T_{HTF} - T_{PCM})/\Phi$, where Φ is the heat flux, T_{HTF} is the average water temperature and T_{PCM} is the average PCM temperature. It is clear that R_t shows a similar behavior for the three cases considered: during the heat conduction regime of the process R_t strongly increases until natural convection starts to affect the melting process. The maximum value of R_t correspond to local minimum value of heat flux that can be observed in Fig. 9 in the very early stage of the process. Thermal resistance decreases during the second stage of the process since heat transfer is augmented by buoyancy driver currents in the liquid PCM. Moreover temperature difference between HTF and PCM decreases. When larger HTF inlet temperatures are considered, the influence of natural convection becomes stronger. As a consequence, it can be observed that the maximum value of R_t decreases of 15% for Case III in comparison to Case I. Once melting is completed thermal resistance strongly increases since heat flux is negligible and PCM temperature approaches HTF inlet temperature.

3.4 Influence of thermal conductivity enhancement

The effect of adding copper powder to the phase change material is addressed by analyzing cases characterized by different particles concentrations. The main goal of this section of the paper is to evaluate system performance improvements accordingly to the current nano-fluid modeling approach which has been described in section 2.2. Consequently, slip conditions between solid particles and basic fluid cannot be included in the analysis. This implies that possible settlement of particles cannot be considered in the problem studied in this paper. Moreover, the focus of this section is only on the thermal behavior of the LHTES unit charged with nano-enhanced PCM. Possible technical problems due to particle sedimentation and thermal cycling are not addressed. Further analysis is planned for the future in order to investigate these aspects of the system.

Previous numerical investigations of nano-enhanced PCM considered large particle volume fractions up to 20% [25], however recently Fan and Kodadadi [28] pointed out that particle settlement can take place in presence of much lower particle concentrations. Therefore, in order to achieve more realistic operating conditions, particle volume fractions of 0.5%, 1%, 2% and 4% are investigated in this paper. Same particle concentrations have been considered in [28,34]. In order to isolate the effect of particle addition, HTF inlet conditions are kept constant when enhanced PCM is considered.

 The liquid fraction of PCM at any time indicates of the progress of the phase change process, thus is worthwhile to analyze it for different particle volume fractions. In Figure 11 the variation of liquid fraction for pure PCM and enhanced PCM is reported. The addition of copper powder considerably enhances the heat transfer: higher liquid fraction at any time is obtained in comparison with pure PCM ($\phi = 0$) The melting time is reduced by 3%, 5%, 9.5% and 15% with particle volume fraction of 0.5%, 1%, 2%, and 4% respectively. Accordingly to Eqs. (7) and (9), energy storage capacity of the LHTES unit is reduced by 0.5%, 1%, 2%, and 4%, with particle volume fraction of 0.5%, 1%, 2%, and 4% respectively.

The influence of thermal enhancement can be seen by analyzing Figure 12: at a given time, melt front position moves downward in the unit as ϕ increases which indicates an increase of melting rate. Furthermore, it can be observed that liquid-solid interface has a similar shape regardless of volume fraction value. This suggests that the buoyancy driven fluid flow preserves it peculiar features also when thermal enhancement is used.

An increase of 16% in the heat transfer rate is achieved with particle volume fraction of 4%. Variation of average heat flux is depicted in Figure 13: heat transfer rate is higher during the near-constant value time range. Later the heat flux drops more rapidly for larger value of ϕ, which again indicates that melting process is faster. Indeed, the addition of particles promotes heat exchange between HTF and PCM in contact with tube wall. Therefore, the addition of nano-particles allows to obtain better performance since heat flux is larger when the unit is usable, that is when heat flux is almost constant. Thus, improved heat transfer between PCM and water allows to use larger LHTES unit (i.e. larger energy storage) with acceptable melting/solidification rates.

From Figure 14 it is possible to observe that in the turbulent regime Re number does not affect the melting process when pure PCM is used. However, if thermal enhancement is considered (Case IX and Case X), a decrease of about 7% in melting time can be observed with larger Re number. This can be explained by the fact that nano-particles allow to decrease PCM thermal resistance which dominates heat transfer process when pure PCM in considered.

4. Conclusions

This paper presented a numerical analysis of PCM melting in a single shell-and-tube LHTES unit. Both conventional PCM and phase change material dispersed with high conductivity nano-particles have been considered. Based on the enthalpy method, the two dimensional axial-symmetric melting process was simulated by means of CFD code FLUENT.

The results indicate that very early stages of the process are dominated by heat conduction and no appreciable fluid flow is established. As liquid PCM fraction increases, buoyancy driven currents are observed and melting rate considerably increases due to the presence of a vortex structure. Melting process is significantly influenced by HTF inlet temperature: the results show that an increase of 15°C of HTF inlet temperature induces an higher heat flux, and consequently a 38% reduction of melting time compared to the initial operating conditions. Such behaviour can be attributed to stronger natural convection which enhances heat transfer between solid PCM and HTF. Indeed maximum value of thermal resistance decreases of 15% when higher HTF inlet temperature is considered. Thus it is possible to conclude that natural convection and inlet HTF conditions greatly affect the thermal fluid-dynamic behaviour of the LHTES unit.

Thermal enhancement by means of nano-particle dispersion has been also investigated in the paper. The numerical results indicate that significant improvements of thermal performance can be achieved. An increase of 16% of heat flux is achieved with particle volume fraction of 4%. This induces a 15% reduction of melting time. When nano-particle enhanced PCM is considered, HTF mass flow rate can affect the phase change process: the simulation shows that melting time diminish of 7% when mass flow rate is doubled.

References

1. Agyenim, F., Hewintt, N., Eames, P., Smyth, M. A review of materials, heat transfer and phase change problem formulation for latent heat thermal energy storage systems (LHTESS), Renewable and sustainable Energy Reviews 2010; 14: 615-628

2. Sparrow E.M., Broadbent J.A., Inward melting in a vertical tube which allows free expansion of the phase-change medium. Journal of Heat Transfer 1982; 104: 309-315.

3. Mennon A.S., Weber M.E., Mujumdar A.S. The dynamics of energy storage for paraffin wax in cylindrical containers. Canadian Journal of Chemical Engineering 1983, 61: 647-653.

4. Jones BJ, Sun B, Krishnan S, Garimella SV. Experimental and numerical investigation of melting in a cylinder. International Journal of Heat and Mass Transfer 2006; 49:2724-38.

5. Zhang Z., Bejan. A. Melting in an enclosure heated at constant rate. International Journal of Heat and Mass Transfer 1989; 32: 1063-1076.

6. Pal D. Joshi Y. K. Melting in a side heated tall enclosure by uniformly dissipating heat source. International Journal of Heat and Mass Transfer 2001; 44: 375-387.

7. Sari A., Kaygusuz, K. Thermal energy storage system using stearic acid as a phase change material. Sol. Energy 2001; 71: 365–376.

8. Keles S., Kaygusuz K., Sari A. Lauric and mystiric acids eutectic mixture as phase change material for low-temperature heating applications. International Journal of Energy Research 2005; 29: 857-870.

9. Ettouney H, El-Dessouky H, Al-Kandari E. Heat transfer characteristics during melting and solidification of phase change energy storage process. Industrial & Engineering Chemistry Research 2004; 43: 5350–5357.

10. Akgun M, Aydin O., Kaygusuz K. Experimental study on melting/solidification characteristics of a paraffin as PCM. Energy Conversion & Management, 2007; 48: 669-678.

11. Aydin O., Akgun M., Kaygusuz K. An experimental optimization study on a tube-in-shell latent heat storage. International Journal of Energy Research 2007; 31: 274-287.

12. Shamsundar N., Sparrow E.M. Analysis of multidimensional conduction phase change via the enthalpy model. Journal of Heat Transfer 1975; 97: 333-340.

13. Voller V.R, Cross M., Markatos N.C. An enthalpy method for convection/diffusion phase change. International Journal for Numerical Methods in Engineering 1987; 24: 271-284.

14. Voller V.R., Prakash C. A fixed grid numerical modeling methodology for convection-diffusion mushy region phase-change problems. International Journal of Heat and Mass Transfer 1987; 30: 1709-1719.

15. Lacroix, L. Numerical simulation of a shell-and-tube latent heat thermal energy storage unit. Solar energy, 1993, 50(4): 357-367.

16. Ismail, K. Abugderah, M. Performance of a thermal storage system of the vertical tube type. Energy Conversion & Management, 2000; 41: 1165-1190.

17. Trp, A. An experimental and numerical investigation of heat transfer during technical grade paraffin melting and solidification in a shell-and-tube latent thermal energy storage unit. Solar Energy 2005; 79:648–660.

18. Ismail K. A. R., Melo C.A. Convection-Based Model for a PCM Vertical Storage Unit. International Journal of Energy Research 1998; 22:1249-1265.

19. Shmueli H., Ziskind G., Letan R. Melting in a vertical cylindrical tube: Numerical investigation and comparison with experiments. International Journal of Heat and Mass Transfer 2010; 53: 4082-4091.

20. Trp A., Lenic K., Frankovic B. Analysis of the influence of operating conditions and geometric parameters on heat transfer in water-paraffin shell-and-tube latent thermal energy storage unit. Applied Thermal Engineering 2006, 26:1830–1839.

21. Bugaje I.M. Enhancing the thermal response of latent heat thermal storage systems. International Journal of Energy Research 1997;21:759–766.

22. Cabeza L.F., Mehling H., Hiebler S., Ziegler F. Heat transfer enhancement in water when used as PCM in thermal energy storage. Applied Thermal Engineering 2002; 22:1141-1151.

23. Pincemina S., R. Olivesa R., Pya X., Christ M. Highly conductive composites made of phase change materials and graphite for thermal storage. Solar Energy Materials & Solar Cells 2008; 92:603–613.

24. Mettawee E.S., Assassa G. M.R.. Thermal Conductivity Enhancement in a Latent Heat Storage System. Solar Energy 2007; 81:839-845.

25. Khodadadi J.M., Hosseinizadeh S.F. Nanoparticle-enhanced Phase Change Materials (NEPCM) with Great Potential for Improved Thermal Energy Storage. International Communication in Heat and Mass Transfer 2007; 34:534-543.

26. Ho C.J., Gao J.Y.. Preparation and Thermophysical Properties of Nanoparticle-in-paraffin Emulsion as Phase Change Material. International Communication in Heat and Mass Transfer 2009; 36:467-470.

27. Seeniraj R.V., Velraj R., Narasimhan N.L. Heat Transfer Enhancement Study of a LHTS Unit Containing Dispersed High Conductivity Particles 2002; 124:243-249.

28. Fan L., Khodadadi J.M. Experimental verification of expedited freezing of nanoparticle-enhanced phase change materials (NEPCM). Proceedings of the ASME/JSME 2011 8th Thermal Engineering Joint Conference. March 13-17, 2011, Honolunu, Hawaii, USA.

29. Khodadadi J.M., Zhang Y. Effects of buoyancy-driven convection on melting within spherical containers. International Journal of Heat and Mass Transfer 2001; 44:1605-1618.

30. H.C. Brinkmann. The viscosity of Concentrated Suspensions and Solutions. Journal of Chemical Physics 1952; 20:571-581.

31. Y. Xuan, W. Roetzel. Conception for Heat Transfer Correlation of Nanofluids. International Journal of Heat and Mass Transfer 2000; 43:3702-3707.

32. Jany P., Bejan A. Scaling theory of melting with natural convection in an enclosure. International Journal of Heat and Mass Transfer 1988; 31: 1221-1235.

33. Adine H., A., El Qarnia, H. Numerical analysis of the thermal behaviour of a shell-and-tube heat storage unit using phase change materials. Applied mathematical modelling, 2009, 33: 2132-2144.

34. S.F. Hosseinizadeh S.F., Rabienataj Darzi A.A,, Tan F.L. Numerical investigations of unconstrained melting of nano-enhanced phase (NEPCM) in a spherical container. International Journal of Thermal Sciences, 2012, 51: 77-83.

35. Akgun M, Aydin O, Kaygusuz K, Thermal energy storage performance of paraffin in a novel tube-in-shell system. Applied Thermal Engineering 2008; 28:405–413.

List of Tables

List of Figures

	PCM	Copper particles
Density ρ [kg/m^3]	794 [10]	8954
Thermal conductivity k [W/(m K)]	0.514 (solid) 0.224 (liquid) [1]	400
Specific heat [J/(kg K)]	2383 (solid) 1929 (liquid) [35]	383
Thermal expansion coefficient β [1/K]	0.00091 [4]	1.67×10^{-5} [25]
Reference Temperature T_0	37.80 [10]	-
Melting temperature range [°C]	37.80 – 44.23 [10]	-
Latent heat [kJ/kg]	249 [35]	-
Nano-particles diameter [nm]	-	15

Table 1. Thermophysical parameters.

	mass flow rate, $\dot{m}_{inlet}$ [kg/min]	Inlet temperature T_{inlet} [°C]	Reynolds number, Re	Rayleigh number, Ra	Stefan Number, Ste	ϕ
Case I	8	60	6044	2.63×10^7	0.15	0
Case II	12	60	9067	2.63×10^7	0.15	0
Case III	16	60	12088	2.63×10^7	0.15	0
Case IV	8	70	6044	4.28×10^7	0.25	0
Case V	8	75	6044	5.10×10^7	0.30	0
Case VI	8	60	6044	2.82×10^7	0.154	0.005
Case VII	8	60	6044	2.87×10^7	0.159	0.01
Case VIII	8	60	6044	2.97×10^7	0.158	0.02
Case IX	8	60	6044	4.07×10^7	0.216	0.04
Case X	16	60	12088	4.07×10^7	0.216	0.04

Table 2. Computational cases studied.
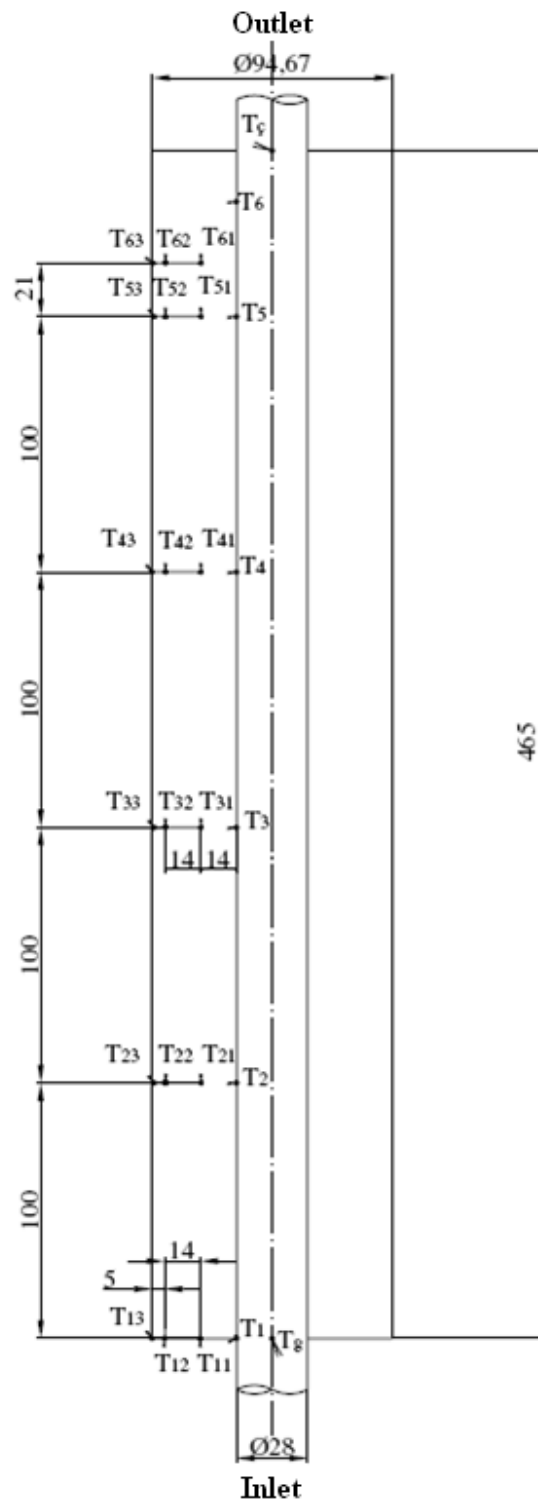
Figure 1. LHTES system geometry and Thermocouples positions [10].
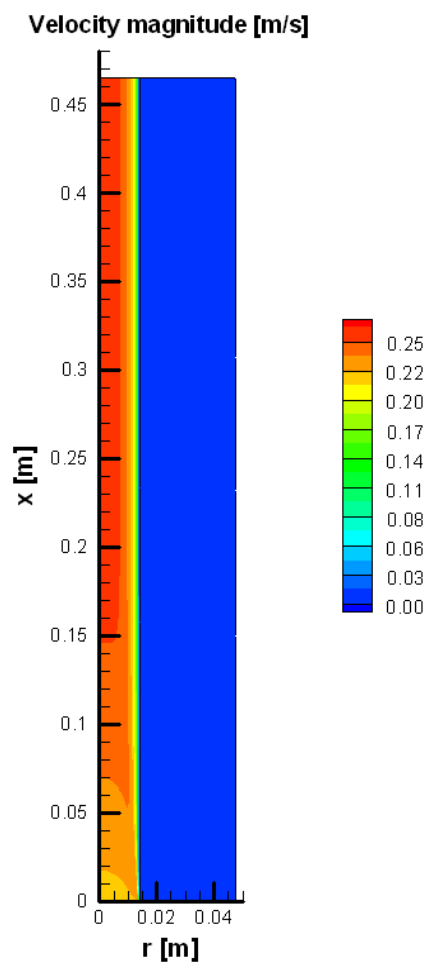
Figure 2. Velocity contours in the HTF pipe. HFT mass flow rate 8 kg/min; Case I.
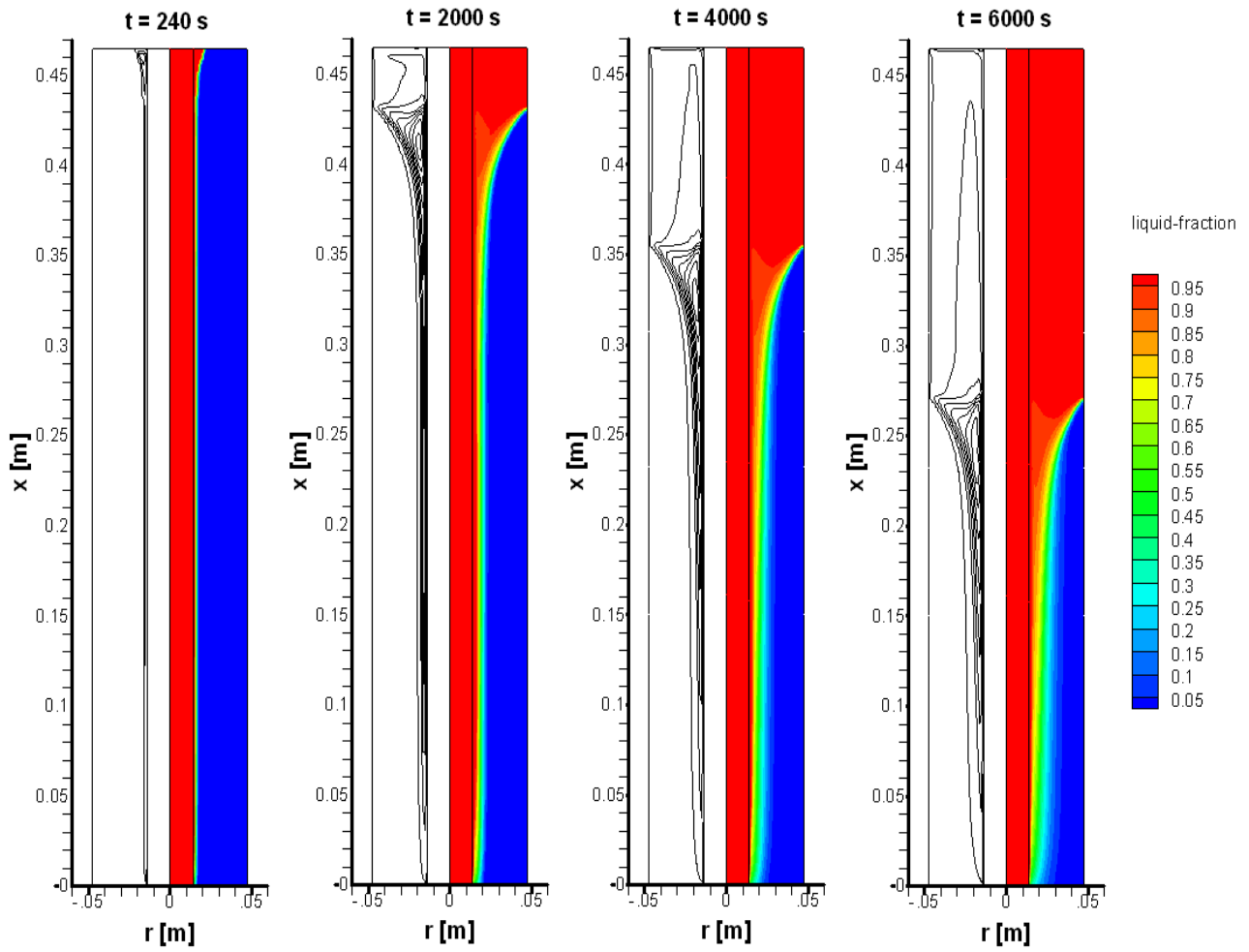
Figure 3. Contours of liquid fraction (right) and streamlines (left). Case I.
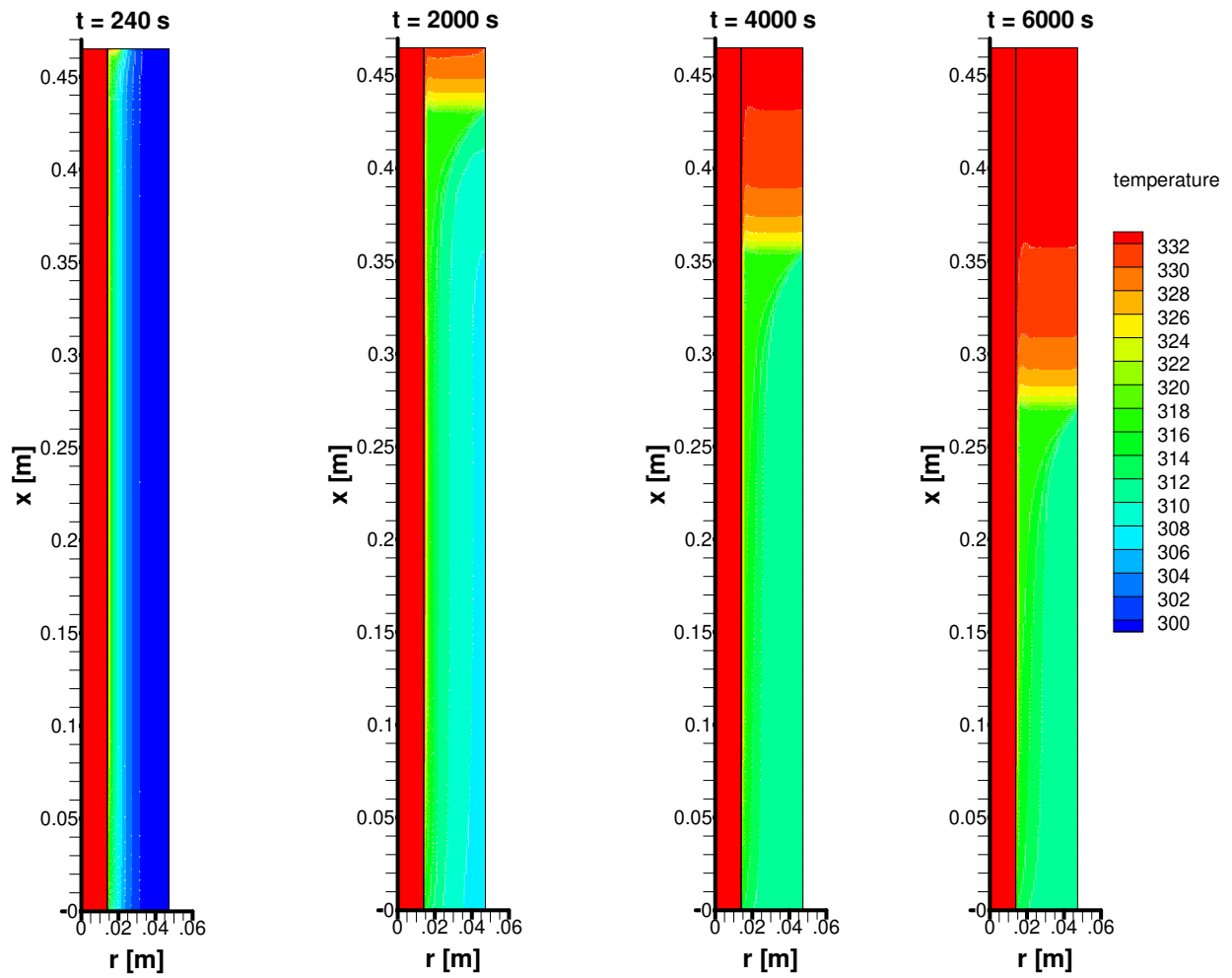
Figure 4. Temperature contours in the HTF and the PCM [K]. Case I.
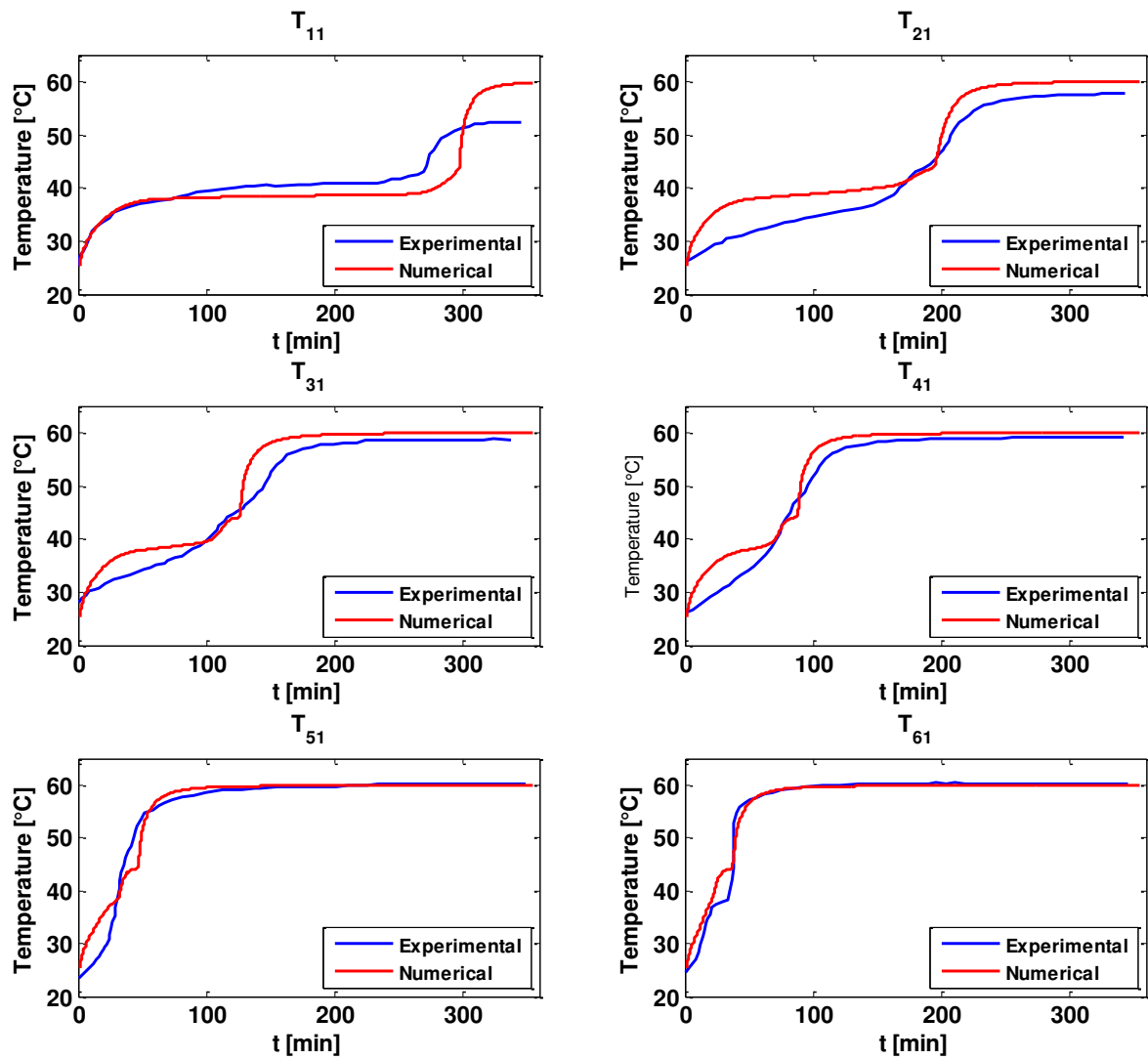
Figure 5. Comparison of computed and experimental temperatures inside the PCM. Case I. Thermocouples locations can be observed in Fig. 1.
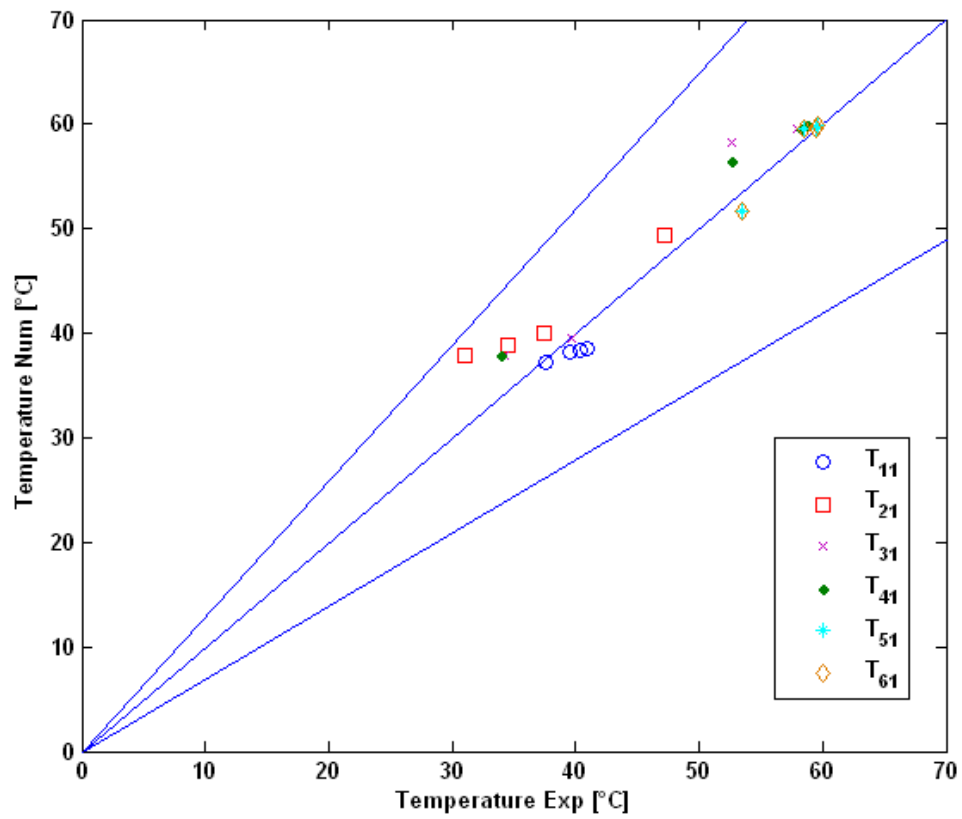
Figure 6. Assessment of the numerical model performance: numerical prediction vs. measurements.
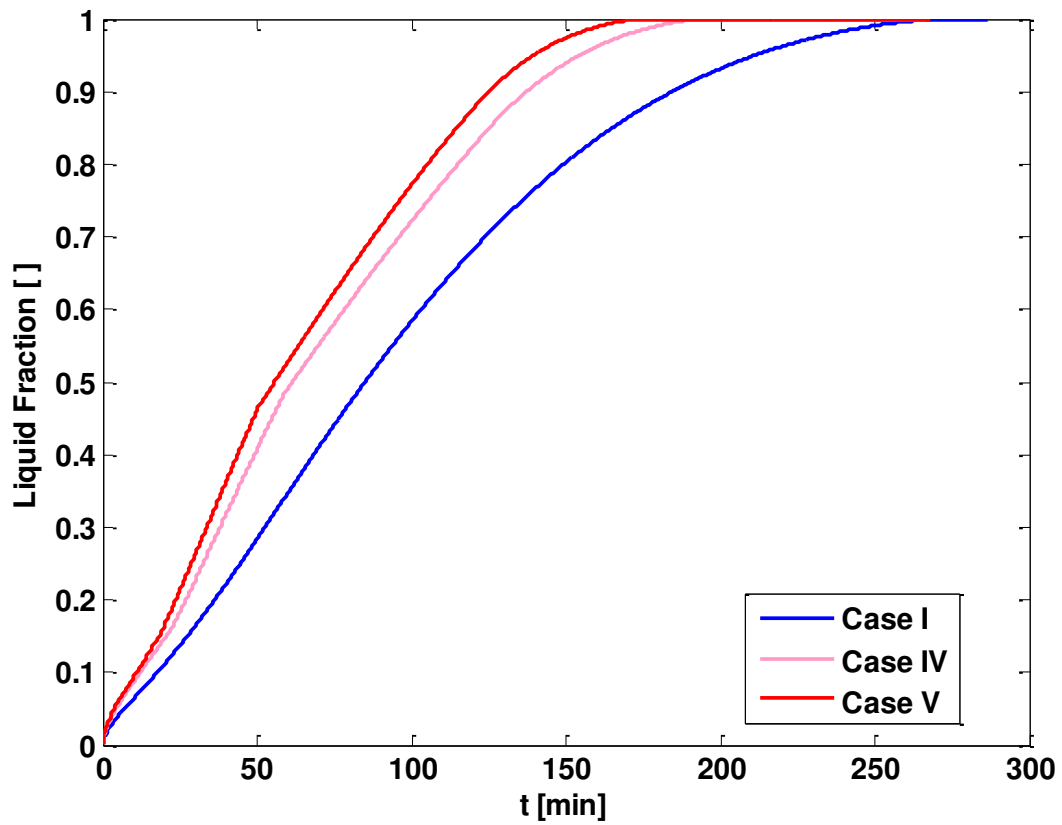
Figure 7. Effect of Ra and Ste number on the temporal evolution of the liquid fraction. Re = 6044.
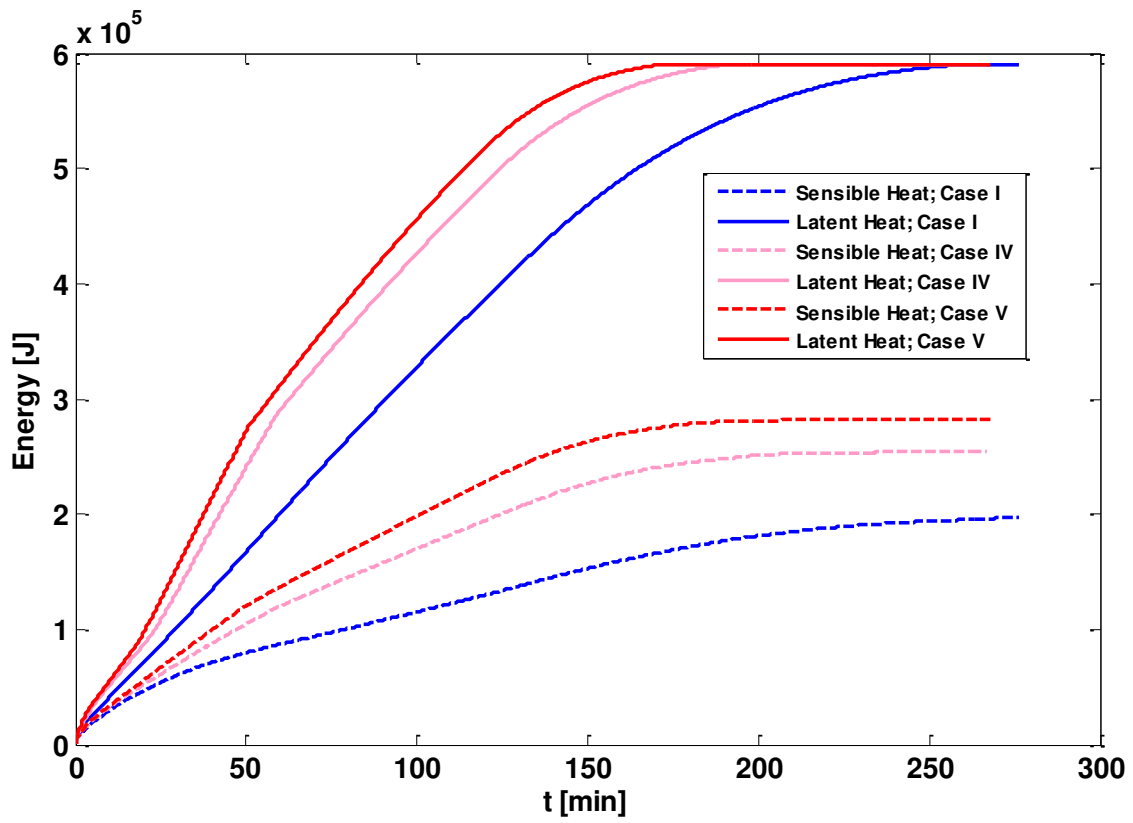
Figure 8. Time wise variation of sensible and latent heat. Re = 6044.
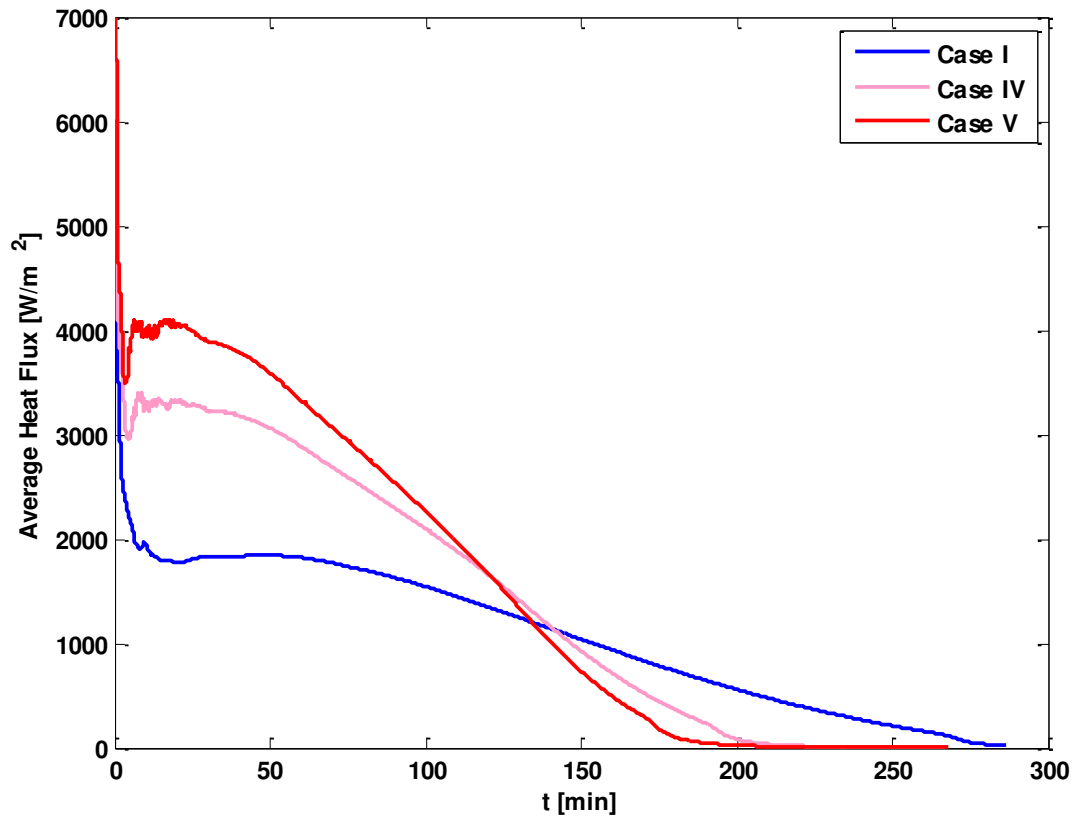
Figure 9. Effect of HTF inlet temperature on average heat flux. Re = 6044.
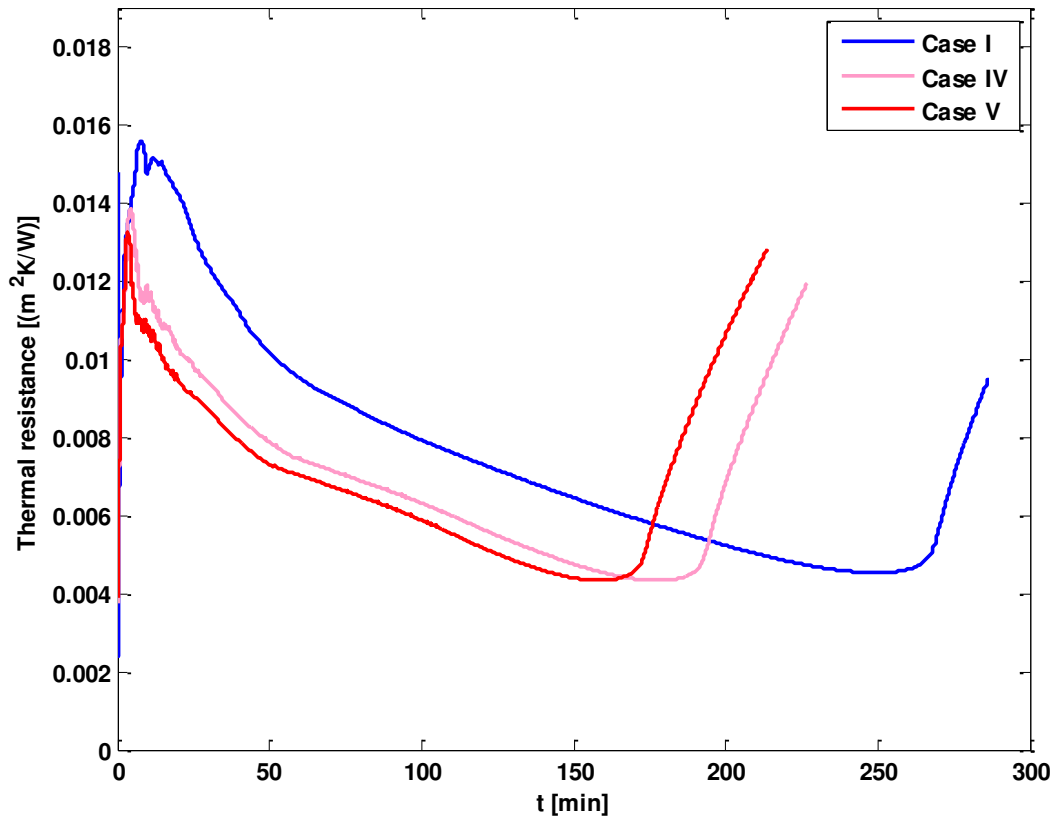
Figure 10. Time evolution of thermal resistance.
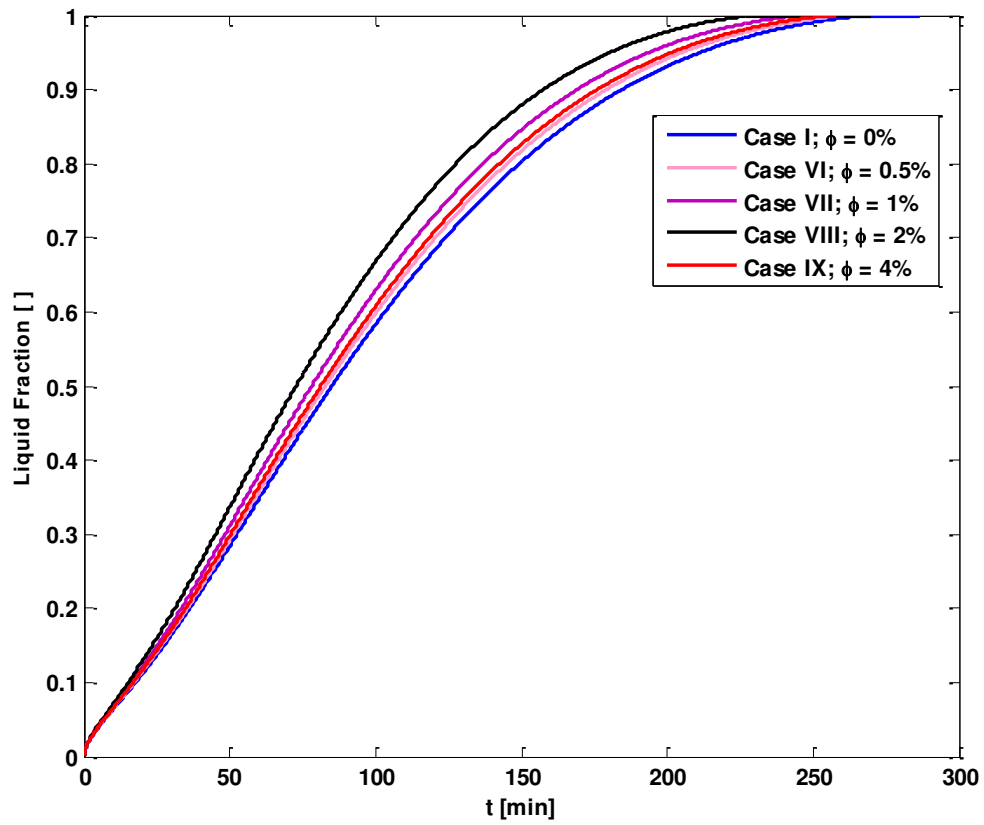
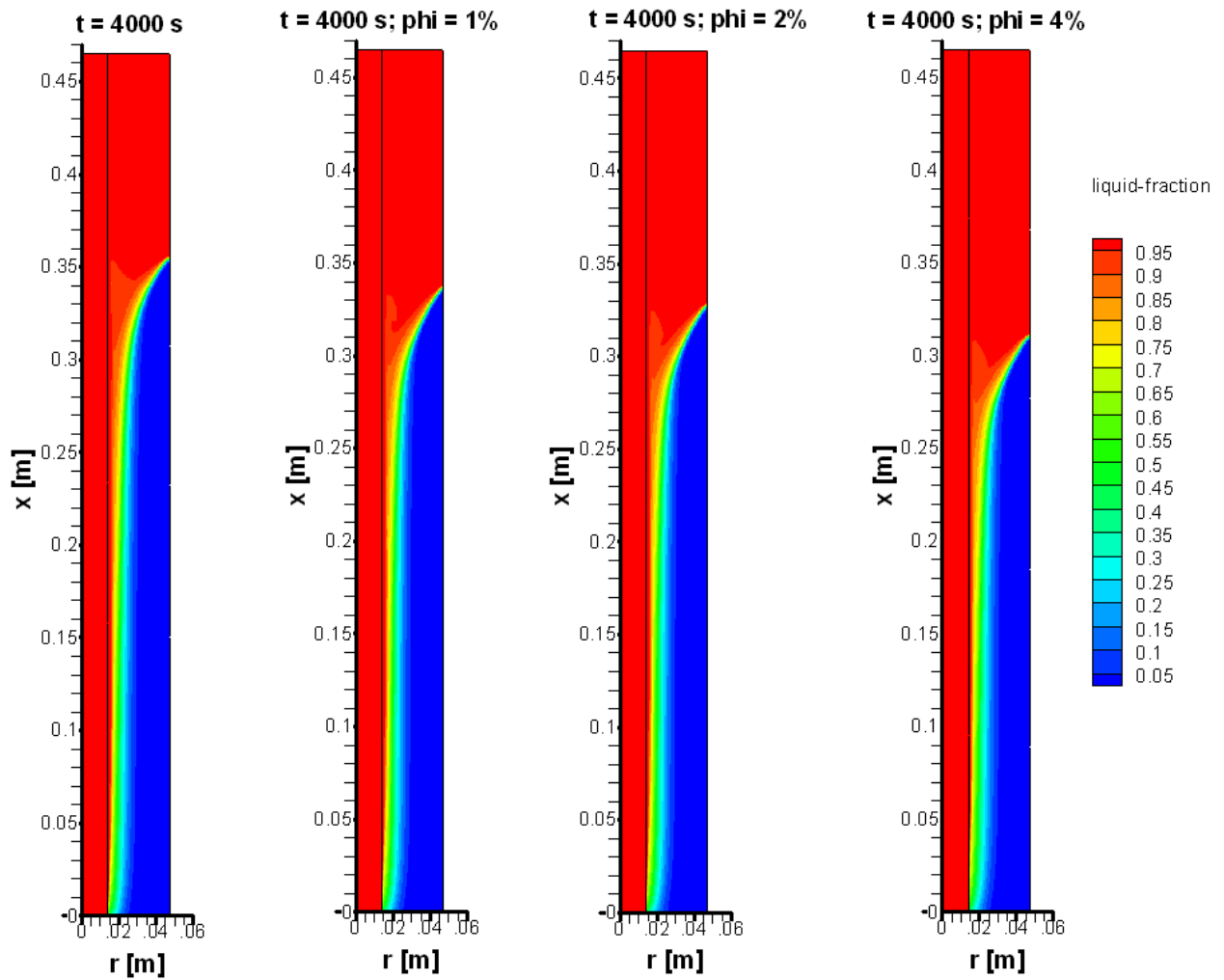**Figure 11. Time evolution of the liquid fraction for various volume fraction of particles.**

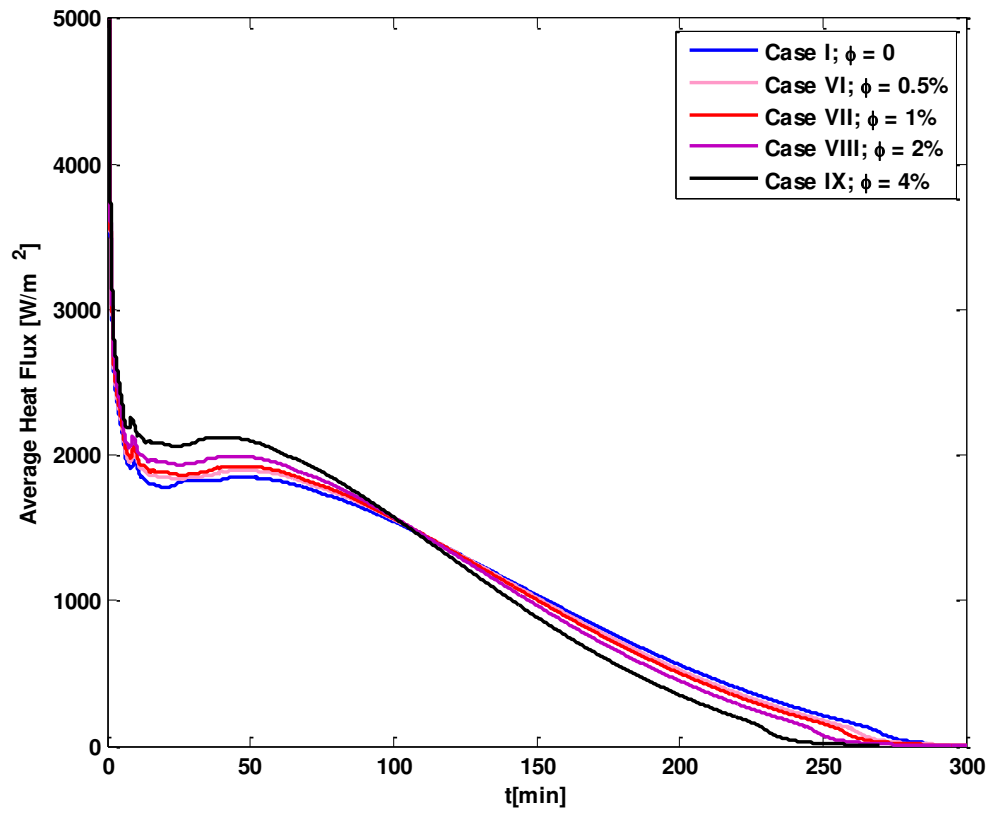**Figure 12. Effect of volume fraction of particles on the instantaneous melt front position.**

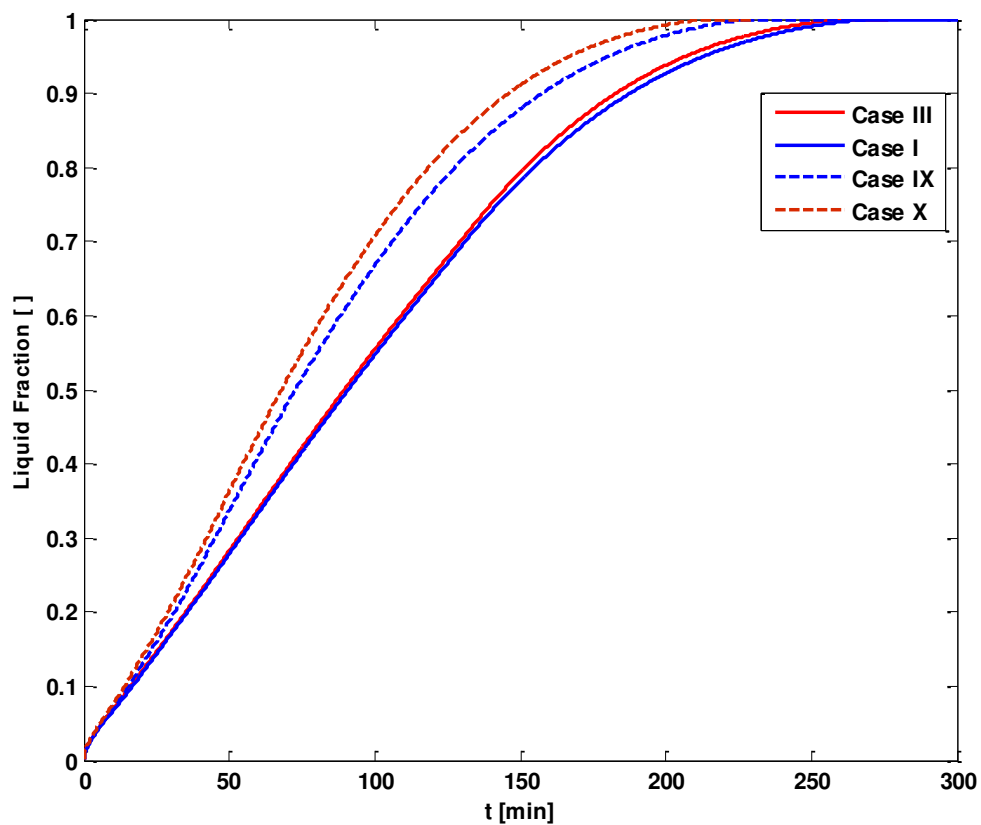**Figure 13. Effect of volume fraction of particles on average heat flux time evolution.**

Figure 14. Effect of Re number on liquid fraction.